

Isovalent dopant-vacancy clusters in silicon: Density functional theory calculations

N. Kuganathan^{a,*}, E.N. Sgourou^b, A. Chroneos^{a,c}, C.A. Londos^b

^a Department of Materials, Imperial College London, London, SW7 2BP, United Kingdom

^b National and Kapodistrian University of Athens, Physics Department, Solid State Physics Section, Panepistimiopolis Zografos, Athens, 157 84, Greece

^c Department of Electrical and Computer Engineering, University of Thessaly, 38221, Volos, Greece

ARTICLE INFO

Keywords:
Silicon
Carbon
Isovalent dopant
Vacancy

ABSTRACT

Isovalent dopants (D) incorporated in the silicon (Si) lattice can readily associate with vacancies to form dopant-vacancy pairs. Theoretical and experimental studies have shown that vacancies (V) tend to accumulate around isovalent dopants to form DV_n clusters, where D is carbon (C) germanium (Ge), tin (Sn) and lead (Pb). Using spin polarised density functional theory, we examine the lowest energy structures of D, DV and VDV (D = C, Ge, Sn and Pb) and the energies to form defects and defect clusters from point defects. The results show that substitution of Ge is thermodynamically favourable. Formation of DV and VDV clusters is endoergic for all dopants. Binding is favourable for all clusters and even more favourable for larger dopants such Sn and Pb. The results are discussed using ionisation energy, structural parameters, Bader charges and electronic structures.

Credit author statement

N. Kuganathan: Methodology, Investigation, Data curation, Writing – original draft. **E.N. Sgourou:** Formal analysis, Validation. **C.A. Londos:** Formal analysis, Writing – review & editing. **A. Chroneos:** Formal analysis, Writing – review & editing.

1. Introduction

Si is the mainstream material used for electronics, photovoltaic applications and a promising semiconductor element for quantum computing [1–6]. Isovalent impurities in Si (i.e. Ge, Sn, Pb and C) of them is that they typically reside on substitutional sites in the Si lattice and they are generally electrically inactive but can introduce lattice strain [7,8].

Ge in Si can suppress the formation of thermal donors, enhance oxygen precipitation, restrain the dislocation movement, increase the mechanical strength of Si and can be used for the manufacturing of void-controlled wafers [7,9–11]. Ge has a slightly larger radius ($r_{\text{Ge}} = 1.22 \text{ \AA}$) than that of Si ($r_{\text{Si}} = 1.17 \text{ \AA}$) and it therefore introduces compressive strains in the Si lattice. To relieve these stains Ge promptly associates with vacancies to form GeV pairs and GeV_n (where n = 1–4) [12–14]. The formation process of the these is Ge → GeV → GeV₂ → GeV₃ → GeV₄.

Clusters like GeV_n and GeV_nO_m were also considered [15,16] to act as heterogeneous nuclei for grown-in oxygen precipitates in Si.

Sn is also a promising isovalent impurity in Si with a covalent radius $r_{\text{Sn}} = 1.41 \text{ \AA}$ that causes significant lattice expansion and drives the formation of Sn-V pairs. As a result the formation of VO and V₂ defects is suppressed, a fact that can improve radiation hardening and modify the mechanical lattice properties of Si material [17–21]. Additionally, Sn reduces the formation of oxygen-related thermal donors and enhance the formation of oxygen precipitates [18,22,23]. However, unlike Ge atom which remains near the V in the GeV pair, the Sn atom in the SnV pair assumes a D_{3d}-symmetric position halfway between two vacancies on adjacent lattice sites [24,25]. Note that SnV pair is infrared inactive and its formation is indirectly deduced by the increase of the VO and V₂ centers concentration as a result of the SnV annealing by dissociation leading to the liberation of V [17,26]. Early studies has indicated [27, 28] that the selective trapping of V by Sn could lead to formation of SnV_n defects through the successive trapping of vacancies by the Sn atom. Additionally, it has been reported that the SnV₂ defect could be formed in the course of irradiation by the direct association of a Sn atom with a V₂ defect [25]. SnV₂ is detected by electron paramagnetic resonance (EPR) and a signal labeled Si-DK1 was related with this. Upon annealing of the latter defect two EPR signal arise in the corresponding spectra labeled Si-DK2 and Si-DK3 attributed to di-tin-divacancy structures

* Corresponding author.

E-mail address: n.kuganathan@imperial.ac.uk (N. Kuganathan).

SnV-SnV and Sn₂V-V respectively observed by EPR [25,26,29–31]. From the technological viewpoint enhanced formation of oxygen precipitation in Si has been attributed [23,32] to the formation of SnV pairs. However, the increase of electrical activity by the formation of Sn-V pairs, due to the introduction of deep levels in the bandgap [33,34] is a negative factor that should be taken into account, since it may restrict the practical usefulness of Sn for radiation hardening of the material. A balance should be maintained between the suppression of the VO and V₂ defects (by Sn doping) and the formation of SnV defects. Notably, the same situation occurs and with the Ge doping since GeV pairs also introduce levels in the gap [35,36].

Pb is the isovalent impurity in Si with the larger covalent radius ($r_{\text{Pb}} = 1, 44 \text{ \AA}$). Its presence at a lattice site induces large compressive strains, the relieve of which results in the formation of PbV pairs. However, any optical or and electrical signal from the above pair has not been definitely reported so far [37,38]. There is, however, indirect evidence for the formation of Pb-V pairs in irradiated Pb-doped Si [39,40]. Due to its large covalent radius Pb competes with O in capturing vacancies and as a result the formation of VO pairs is suppressed substantially [40]. Clearly, in a larger percentage than that in Sn-doped Si. It has been reported [40] that PbV pairs do not dissociate below 280 °C. Theoretical studies [37, 41–43] have reported that Pb processes a split vacancy configuration where the Pb atom occupies the position between two vacancies. It has been found that the Pb dopant in Si suppress the density of growth of micro defects, affects the recombination parameters of the material, increase the carrier's lifetime, influence the concentration of dislocations as well as the formation of thermal donors and oxygen precipitates [38,44,45]. Importantly, the presence of Pb in the Si lattice does not induce the formation of defects in the as-grown material [39]. Pb in Si is commonly introduced with the smaller C as co-dopant to relieve the strains. C has been used to retain Pb atoms at substitutional sites and to inhibit the formation of Pb precipitates [44–48].

C is the isovalent impurity in Si with the smaller covalent radius ($r_{\text{C}} = 0.77 \text{ \AA}$). Due to its smaller size compared to Si it introduces tensile strains in the lattice which lead to its preferential association with self-interstitials. As a result C incorporation in the lattice affects the balance between intrinsic defects that is vacancies and self-interstitials [49,50]. C affects the formation of thermal donors and oxygen precipitates [7, 51–53]. C is commonly used as a co-dopant with Ge, Sn and Pb in Si material processing [27,38,47,54–56]. The issue of a carbon-vacancy center in Si has been considered in the literature but the picture is still not clear. Early theoretical calculations has concluded either in favor [57] of the formation of a CV pair, or against [58] its formation. Recent theoretical calculations [59] have reported two IR bands at 705 and 716 cm⁻¹ associated with the C₈V pair. Experimentally, there are a lot of works making tentative assignments of various signals to C-V structures. For instance broad line in the range of 704–735 cm⁻¹ has been correlated [60] with C-V centers. This outcome is in agreement with the value calculated in ref. 59. Additionally there is reports considered [61–63] the formation of CV structures. A strong experimental argument in favor of the CV center formation is that there are a lot pairs of vacancies with dopants [64] as B, Al, Ga, In, N, P, As, Sb, O as well as with isovalent impurities [7,39,40] as Ge, Sn, Pb which support the expectation of the existence of CV pairs. Thus, the study of CV_n clusters is expected to provide information that would be useful for the Si material technology.

In this study, spin polarised density functional theory (DFT) was employed to find the lowest energy structures of substitutional (D), substitutional-vacancy (DV) and vacancy-substitutional-vacancy (VDV) (D = C, Ge, Sn and Pb) in Si together with their electronic structures and calculate the formation and binding energies of clusters from D and V.

2. Computational methodology

For all the calculations throughout this study, we used a plane wave DFT code VASP (Vienna Ab initio Simulation Package, version 5.3.5) [65]. This code includes projected augmented wave (PAW) potentials

[66] and plane wave basis sets. A plane wave basis set with a cut-off energy of 500 eV was set to all calculations. The valence electronic configurations of C, Si, Ge, Sn and Pb were 2s²2p², 3s²3p², 4s²4p², 5s²5p² and 6s²6p². The exchange correlation term was modelled using the generalised gradient approximation (GGA) parameterised by Perdew, Burke and Ernzerhof (PBE) [67]. Defect structures were modelled using a supercell consisting of 250 Si atoms with the lattice parameters: a = b = c = 19.27 Å. The bulk Si and supercell structures were sampled by using 8 × 8 × 8 and 4 × 4 × 4 Monkhorst-Pack [68] k-point meshes respectively. Full relaxation (positions and lattice constants) was performed using the conjugate gradient algorithm [69] to obtain energy minimum structures. Force tolerance was set to 0.001 eV/Å. Accuracy for electronic minimization was set to 10⁻⁴ eV. Substitutional doping energy for a single dopant atom (D = C, Ge, Sn and Pb) in the Si supercell was calculated using the following equation.

$$E_{\text{sub}} = E_{\text{D} \bullet \text{Si_supercell}} + E_{\text{Si}} - E_{\text{Si_supercell}} - E_{\text{D}} \quad (1)$$

where $E_{\text{D} \bullet \text{Si_supercell}}$ is the total energy of a single dopant atom to replace a single Si atom in the Si supercell, $E_{\text{Si_supercell}}$ is the total energy of the Si supercell and E_{Si} and E_{D} are the total energies of a single Si and D atoms in their bulk structures (or single atomic gas phases) respectively. The following equation was used to calculate the formation energy of a DV defect cluster.

$$E_f(\text{DV}) = E_{\text{DV_supercell}} + 2 E_{\text{Si}} - E_{\text{D}} - E_{\text{Si_supercell}} \quad (2)$$

where $E_{\text{DV_supercell}}$ is the total energy of a Si supercell containing DV defect cluster.

The binding energy of a DV cluster was calculated using the following equation.

$$E_b(\text{DV}) = E_{\text{DV_supercell}} + E_{\text{Si_supercell}} - E_{\text{D} \bullet \text{Si_supercell}} - E_{\text{Si_supercell}} \quad (3)$$

where $E_{\text{Si_supercell}}$ is the total energy of a supercell consisting of a Si vacancy.

Cohesive energies were calculated using the following equation:

$$E_{\text{coh}}(M = \text{C, Ge, Sn and Pb}) = E_M^{\text{isolated}} - E_M^{\text{bulk}}, \quad (4)$$

where E_M^{isolated} and E_M^{bulk} are the total energies of an isolated gas phase M atom and the M atom in the bulk, respectively.

Bader charge analysis [70] was used to estimate the charges on the doped atoms and the Si atoms bonded to them.

3. Results and discussion

3.1. Structural modelling of Si

The crystal structure of Si is cubic, belonging to the space group Fd 3m (No: 227), with unit cell parameters a = b = c = 5.32 Å (see Fig. 1a). Fully relaxed configuration yielded a value of 5.35 Å which is in close agreement with the values reported in the experiment [71], showing the efficacy of the pseudopotentials and basis sets used in this study. The calculated band gap (0.60 eV) is smaller than the value reported in the experiment (1.17 eV) [72] and reasonable agreement with the values reported in other DFT simulation studies [73,74] (see Fig. 1b).

3.2. V and VV defects

The formation energies of a single and a di-vacancy defect were calculated. The formation of a single vacancy is endoergic and the calculated formation energy is 3.63 eV. The formation energy of the di-vacancy cluster is 5.34 eV. The cluster binding energy was calculated to predict the stability of this cluster forming from two isolated vacancy defects. The calculated binding energy is -1.92 eV. This indicates that the defect cluster is more stable than the isolated vacancy defects.

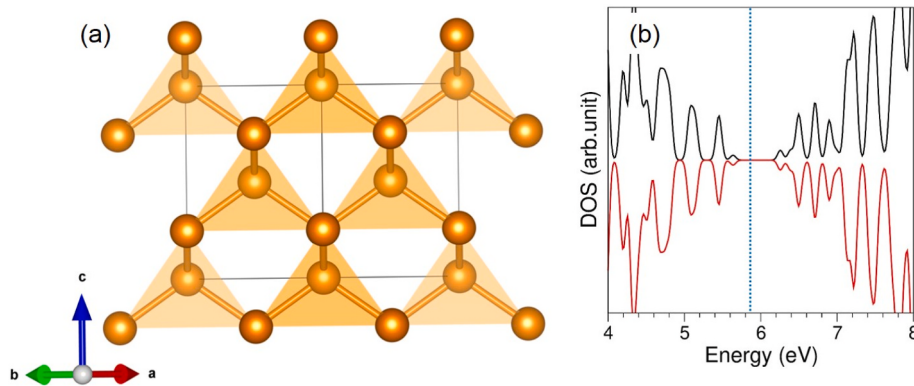


Fig. 1. (a) Relaxed structure of bulk Si and (b) its DOS plot. Blue vertical dot lines correspond to the Fermi energy level.

3.3. D-doped silicon

Relaxed structures of single substitutional D ($D = C, Ge, Sn$ and Pb) atoms in Si are shown in Fig. 2(a-d). In the optimised configurations, a tetrahedral coordination between the dopant and the nearest neighbour Si atoms is observed for all four dopants [see Fig. 2e-h]. In the CSi_4 tetrahedral unit, C-Si bond distances are shorter than the D-Si bond distances ($D = Ge, Sn$ and Pb) found in the DSi_4 units. This is due to the atomic radius of C (1.90 \AA) smaller than that of Si (2.32 \AA) [75]. The shortest C-Si bond distance leads to the formation of strongest bond between the C and Si as evidenced by the largest ionisation energy difference between them (C: 11.26 and Si: 7.89) [76]. The larger ionisation energy of Si results in the positive Bader charge of $\sim +1.00$ each on the four nearest neighbour Si atoms. Accumulation of positive charges on the Si atoms is compensated via gaining of ~ 4 electron by the substitutional C. Energy to substitute a single C atom is 0.44 eV indicating this process not favourable (see Table 1). There is a small contraction of volume upon C doping. This is associated with the contraction of C-Si bond distance with respect to Si-Si bond distance (2.37 \AA) in the pristine Si lattice. In the case of Ge, substitution is favourable and its substitution energy is -0.08 eV with respect to bulk Ge as a reference state. Such favourability is partly due to the atomic

radii of Si and Ge closer to each other (Si: 2.32 \AA and Ge: 2.34 \AA) [75] and the small ionisation energy difference between Si and Ge (Si: 8.15 and Ge: 7.89) [76]. Substitution is favourable for C with respect the gas phase atom as a reference state. Substitution energy is -2.78 eV . Substitution energy increases gradually with increasing atomic radius. Larger cohesive energy of C than that of Ge results in its unfavourable substitution. The Ge-Si bond distance (2.41 \AA) is closer to the Si-Si bond distance. This is further supported by the smaller volume change ($+0.08\%$). A small polarisation is noted in the $GeSi_4$ tetrahedral unit as evidenced by the small Bader charges on Ge and Si atoms. Lower ionisation energy of Ge leads to the positive charge on it and leaves the nearest neighbour Si atoms partially negative. Substitution of Sn and Pb is endothermic. Larger atomic radius of Pb reflects in its larger substitution energy than that calculated for Sn. Ionisation energies of Sn and Pb are smaller than that of Si leaving Sn and Pb highly positive and the nearest neighbour Si atoms negatively charged. Larger Sn (or Pb)-Si bond distance reflects in the larger volume expansion compared to that observed in the Ge doping.

Total DOS plots show that the doped configurations are still semiconductors [see Fig. 3(a-d)]. The p -states of all dopants lie in the valence band and strongly mixed with the states of Si [see Fig. 3(e-h)]. Charge density plot of associated with the C-substitution shows the

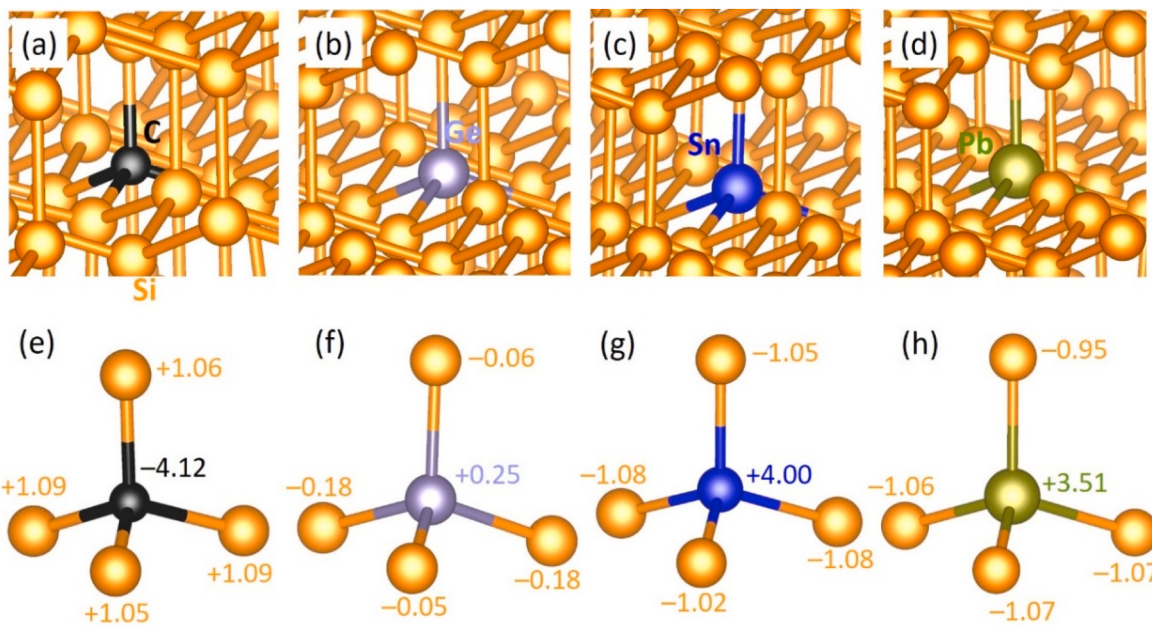


Fig. 2. Relaxed structures of a single (a) C, (b) Ge, (c) Sn and (d) Pb substitutionally doped in Si. Corresponding dopants forming tetrahedral units (e-h) with nearest neighbour Si atoms and the Bader charges on them are also shown.

Table 1

Calculated cohesive energy, substitution energy, Bader charges on substitutionals, Si-D bond distances and volume changes on doping. Substitution energy calculated using gas phase atom as a reference state is given in parentheses.

Dopant (D)	Atomic radius (\AA) [11]	Ionisation energy (eV) [12]	Cohesive energy (eV)	Substitution energy (eV)	Bader charge on D (e)	Si-D (\AA)	$\frac{\Delta V}{V} \times 100$ (%)
C	1.90	11.26	7.81	0.44 (-2.78)	-4.12	2.02	-0.40
Ge	2.34	7.89	3.58	-0.08 (0.93)	+0.25	2.41	+0.08
Sn	2.48	7.34	3.10	0.58 (2.07)	+4.00	2.55	+0.26
Pb	2.49	7.42	2.99	1.58 (3.18)	+3.51	2.61	+0.31

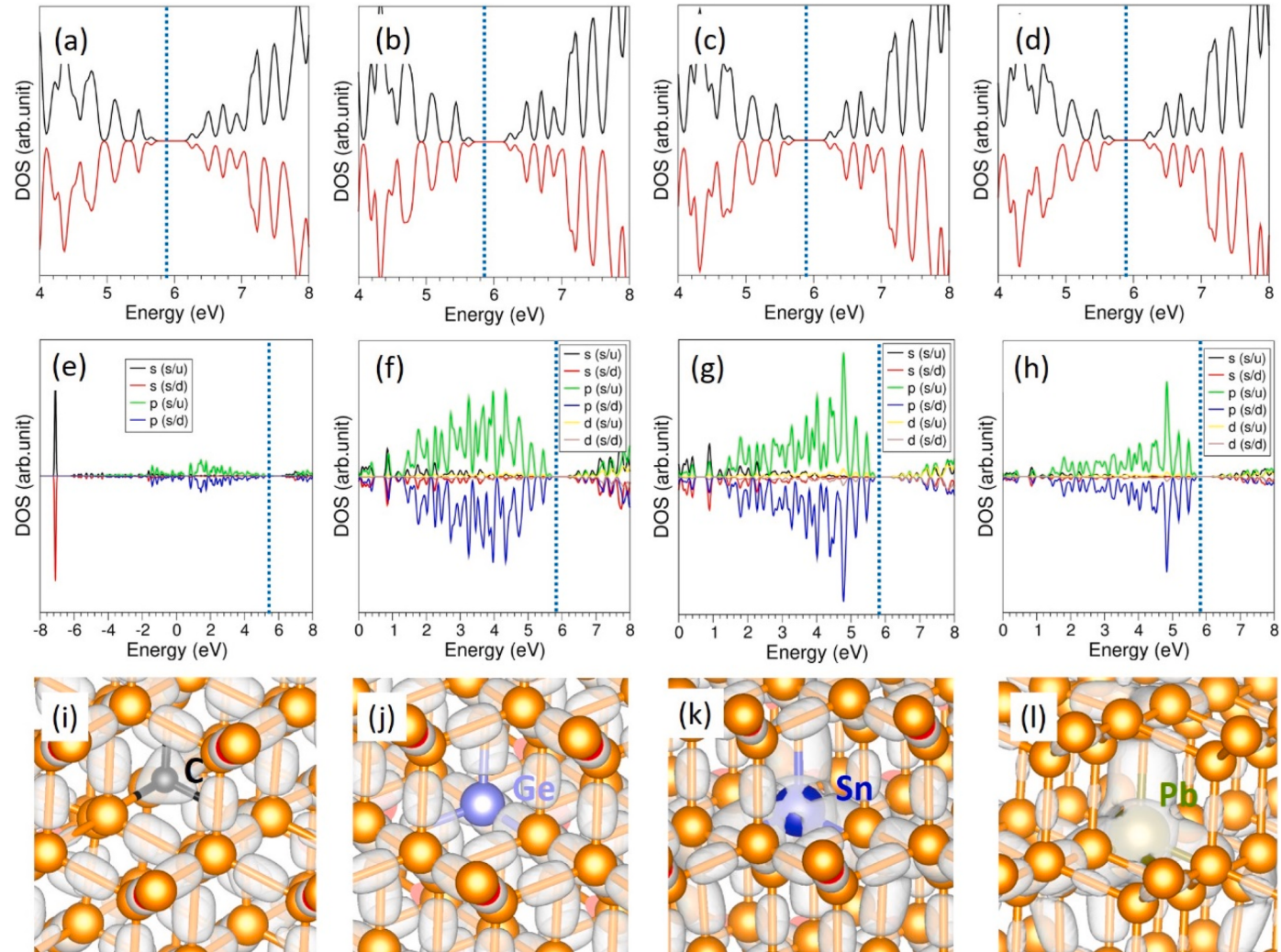


Fig. 3. Total DOS plots of a single (a) C, (b) Ge, (c) Sn and (d) Pb substitutionally doped in Si. Corresponding atomic DOS plots (e–h) and charge density plots (i–l) associated with the states near the Fermi energy level are also shown.

accumulation of electrons on the C as evidenced by the negative Bader charge. In the case of Ge, electron density is absent on it in line with the small positive Bader charge of +0.25. For both Sn and Pb, the charge density is more delocalised between the Si atoms and dopant atoms. In all four doped configurations, the net magnetic moments were found to be zero.

3.4. DV defect

Next, we considered a single substitutional atom and a pre-existing Si vacancy in the supercell. The relaxed structures of the most stable DV configurations are shown in Fig. 4(a–d). In the electronic supplementary information, we provide different DV configurations together with their relative energies (see Fig. S1). In the relaxed structures, dopants form

three coordinated environment with three nearest neighbour Si atoms [see Fig. 4(e–h)]. The substitutional C atom forms a distorted trigonal planar structure consisting of three identical bond angles of 118.2° and bond lengths of 1.88 Å (see Fig. 4a). The presence of vacancy has reduced the C-Si bond length by 0.14 Å. For the other dopants, a distorted trigonal pyramid structure is formed between dopants and three nearest neighbour Si atoms [see Fig. 4(b–d)]. The Bader charge on the Ge is +0.13. The Si atoms bonded to it are slightly polarised. While Si-Ge-Si bond angles are contracted, the Si-Ge bond lengths are slightly expanded (see Table 2). A significant change in bond lengths and angles is noted. This is partly owing to the positive Bader charges on both Sn and Pb arising from their lower ionisation energies compared to that of Si. In all cases, there is a reduction in the volume. The larger volume reduction is noted for C. Contraction of volume is reinforced by the

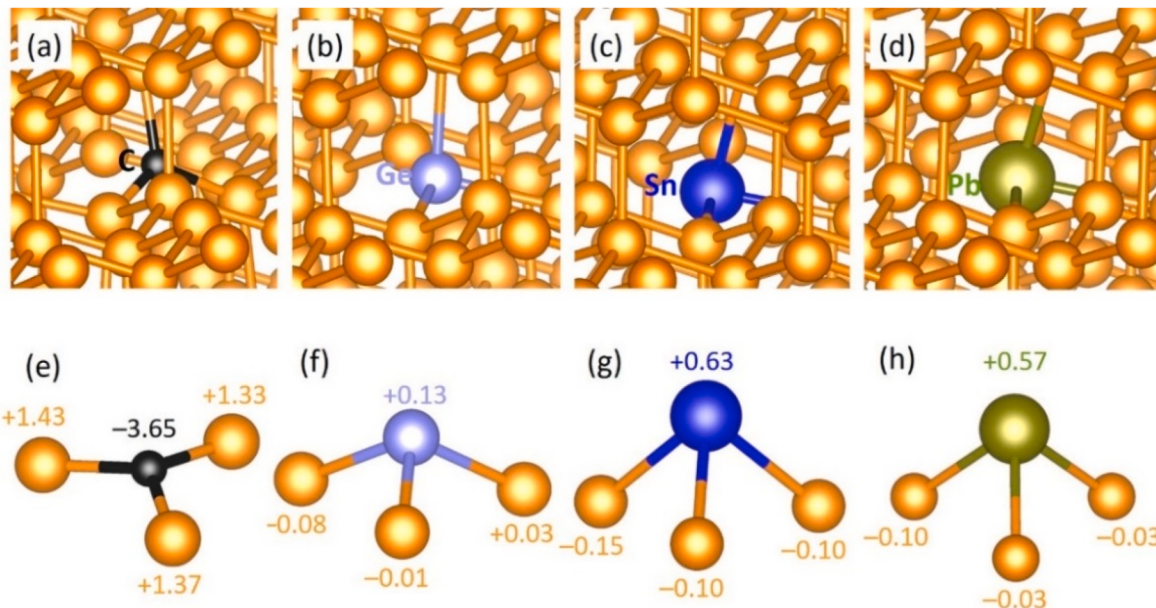


Fig. 4. Relaxed structures of (a) CV, (b) GeV, (c) SnV and (d) PbV defect clusters (a–d) in Si. Corresponding dopants forming three coordinated structures (e–h) with nearest neighbour Si atoms and the Bader charges on them are also shown.

Table 2

Formation energy, binding energy, Bader charges on substitutional atoms, Si-D bond distances and volume changes on doping. Formation energy calculated using gas phase atom as a reference state is given in parentheses.

Dopant (D)	Formation energy (eV)/defect	Binding energy (eV)/defect	Bader charge on D (e)	Si-D (Å)	Si-D-Si (°)	$\Delta V \times 100 (\%)$
C	1.85 (2.54)	-0.18	-3.65	1.88	118.2 (3)	-0.48
Ge	1.65 (4.45)	-0.12	+0.13	2.48	101.4 (3)	-0.27
Sn	1.43 (4.47)	-0.67	+0.63	2.87	84.1 (3)	-0.21
Pb	1.75 (4.85)	-0.85	+0.57	2.94	83.8 (3)	-0.07

expansion of bond distance from C to Pb. Energy to form DV cluster is endothermic in all cases. The formation of the CV cluster is slightly more unfavourable than others. Binding energy to form DV cluster from isolated defects (D and V) was calculated. In all cases, exothermic binding is observed. This indicates that there is a strong tendency to form cluster from point defects. Formation energies calculated using gas phase atoms as reference states are highly positive compared to those calculated using atoms in their bulk structures as reference states. In this case, formation energy increases with increasing atomic radius. The lowest binding energy was calculated for GeV cluster although the binding energy is -0.12 eV. The binding energy of PbV cluster is highly exothermic with a binding energy of -0.85 eV.

The inclusion of vacancy leads to the mixing of p -states of dopants and electrons near the Fermi energy level and brings the band gap down [see Fig. 5(a–h)]. The charge density plots associated with the states near the Fermi energy level shows that electron density is localised near the vacancy and the dopant [see Fig. 5(i–l)]. A zero magnetic moment was noted in all optimised configurations.

3.5. VDV defect

Finally, we considered a cluster consisting of two vacancies and a substitutional D. We provide different VDV configurations together with

their relative energies in the ESI (see Fig. S2). The relaxed structures are shown in Fig. 6(a–d). A distorted trigonal planar arrangement is noted for C as observed in the CV defect configuration (see Fig. 6e). A distorted trigonal pyramid structure is predicted for the other VDV clusters [see Fig. 6(f–h)]. Formation of VDV clusters is endothermic in all cases and energy to form clusters per defect is not altered much compared to that calculated for DV clusters. Formation of VSnV is more favourable than that of other clusters. High positive formation energies are calculated using gas phase atoms as reference states and there is a gradual increase in the formation energies with increasing atomic radius. Binding energies are negative in all cases (see Table 3). The calculated values are more exothermic than that calculated for DV clusters. Again as noted in the binding of DV clusters, binding of VPbV cluster from two V and Pb isolated defects is the lowest energy process. The Si-D bond distance increases with increasing atomic radius. Conversely, Si-D-Si bond angle decreases from C to Pb. Contraction of volume is noted in all cases and becomes smaller with increasing atomic radius.

The total DOS plots show that the resultant VDV cluster configurations exhibit metallic character [see Fig. 7(a–d)]. The p -states of dopants are localised in the valence band and near the Fermi energy level [see Fig. 7(e–h)]. Charge density plots associated with the states near the Fermi energy level are shown in Fig. 7(i–l). Electron density is localised mainly near the vacancies and the dopants. Non-magnetic configurations were found in all cases.

All the defect clusters considered are bound and important as it has been demonstrated in dopant-vacancy clusters in Si and related systems [77–79]. Kinetics and processing conditions (i.e. annealing, irradiation or implantation) will play a role and will impact the formation of these dopant-vacancy clusters at significant concentrations [80,81].

3.6. Impact of vacancies on the doping process

The effect of doping with and without vacancies was considered. Table 4 shows the reaction energies. For all four dopants, a single vacancy defect has reduced the cost of doping. The presence of di-vacancy has reduced the substitution energy for C and Ge. For Sn and Pb, the doping process with di-vacancy is slightly more endoergic than that with a single vacancy.

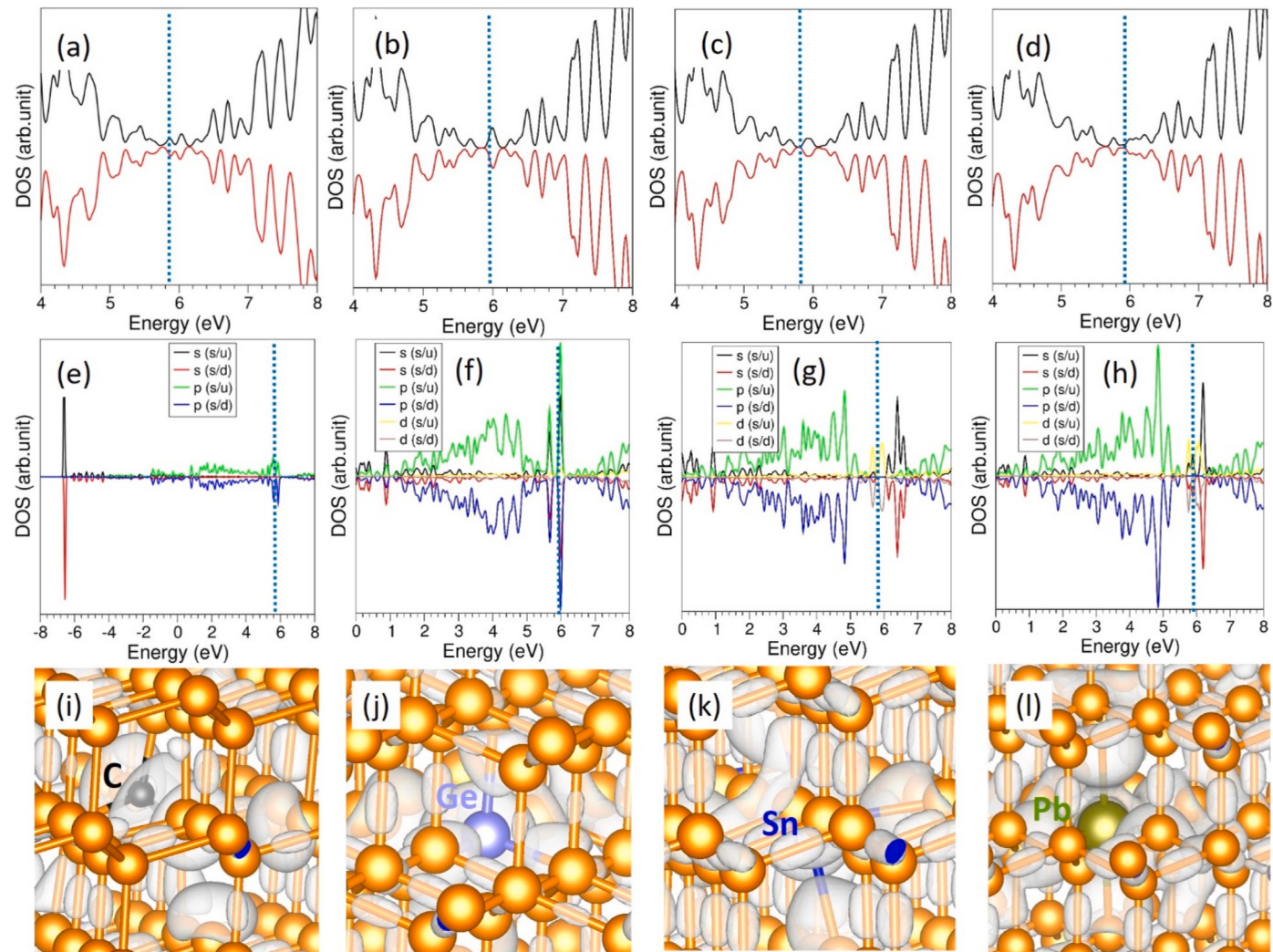


Fig. 5. Total DOS plots of (a) CV, (b) GeV, (c) SnV and (d) PbV defect clusters in Si. Corresponding atomic DOS plots (e–h) and charge density plots (i–l) associated with the states near the Fermi energy level are also shown.

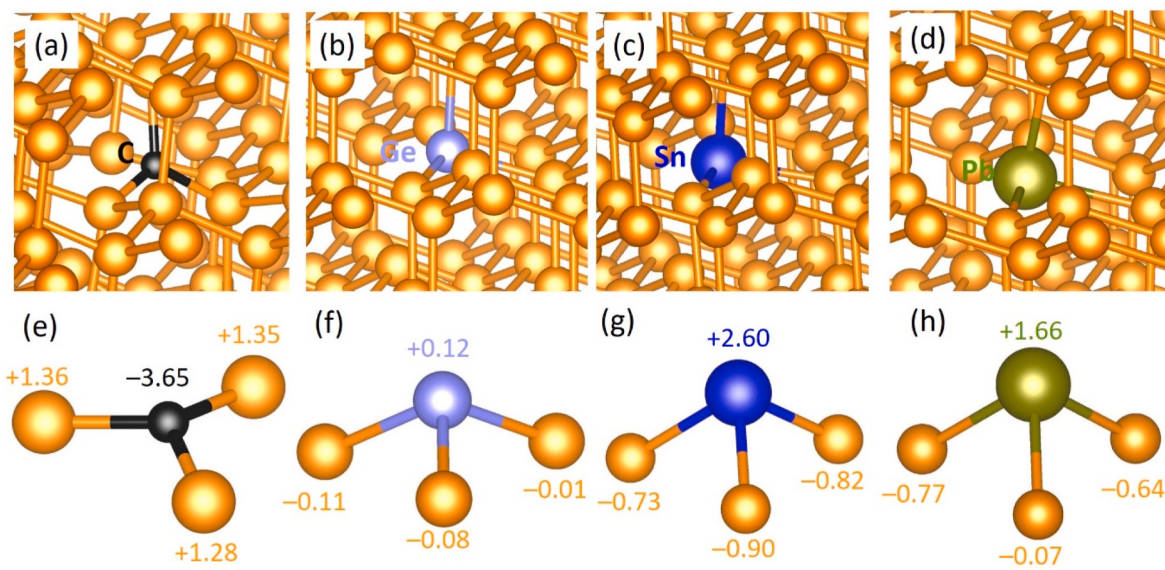


Fig. 6. Relaxed structures of (a) VCV, (b) VGeV, (c) VSnV and (d) VPbV defect clusters (a–d) in Si. Corresponding dopants forming three coordinated structures (e–h) with nearest neighbour Si atoms and the Bader charges on them are also shown.

Table 3

Formation energy, binding energy, Bader charges on substitutionals, Si-D bond distances and volume changes on doping. Formation energy calculated using gas phase atom as a reference state is given in parentheses.

Dopant (D)	Formation energy (eV)/defect	Binding energy (eV)/defect	Bader charge on D (e)	Si-D (Å)	Si-D-Si (°)	$\frac{\Delta V}{V} \times 100$ (%)
C	1.75 (3.74)	-0.81	-3.64	1.88 (3)	115.9 (1), 119.4 (2)	-0.84
Ge	1.67 (5.06)	-0.72	+0.12	2.44, 2.48 (2)	99.4 (1), 103.3 (2)	-0.49
Sn	1.58 (5.14)	-1.03	+2.60	2.65, 2.75 (2)	89.0 (1), 93.9 (2)	-0.41
Pb	1.79 (5.39)	-1.15	+1.66	2.75, 2.85 (2)	87.5 (2), 95.9 (2)	-0.33

5. Conclusions

The standard process of manufacturing Si-based electronic devices involves thermal treatments which entail the inevitable formation of thermal donor and oxygen precipitates. These defects affect the quality of the wafer and their control is very important. On the other hand, we have seen that isovalent impurities influence the formation of thermal donors and oxygen precipitates. DV_n ($D = C, Ge, Sn$, and Pb) defects play an important role in these processes. The detailed study of the structure and properties of the DV_n defects will provide additional information to improve the functionality of the devices.

Table 4

Reaction energy calculated for the doping in the absence and presence of vacancies.

Reaction	Reaction energy (eV)				
	Dopant (D)	C	Ge	Sn	Pb
$Si_{supercell} + D \rightarrow D:Si + Si$	-2.78	0.93	2.07	3.18	
$V_{Si} + D \rightarrow D:V_{Si} + Si$	-3.14	0.68	0.72	1.48	
$V_{Si}V_{Si} + D \rightarrow D:V_{Si}V_{Si} + Si$	-3.30	0.60	0.90	1.64	

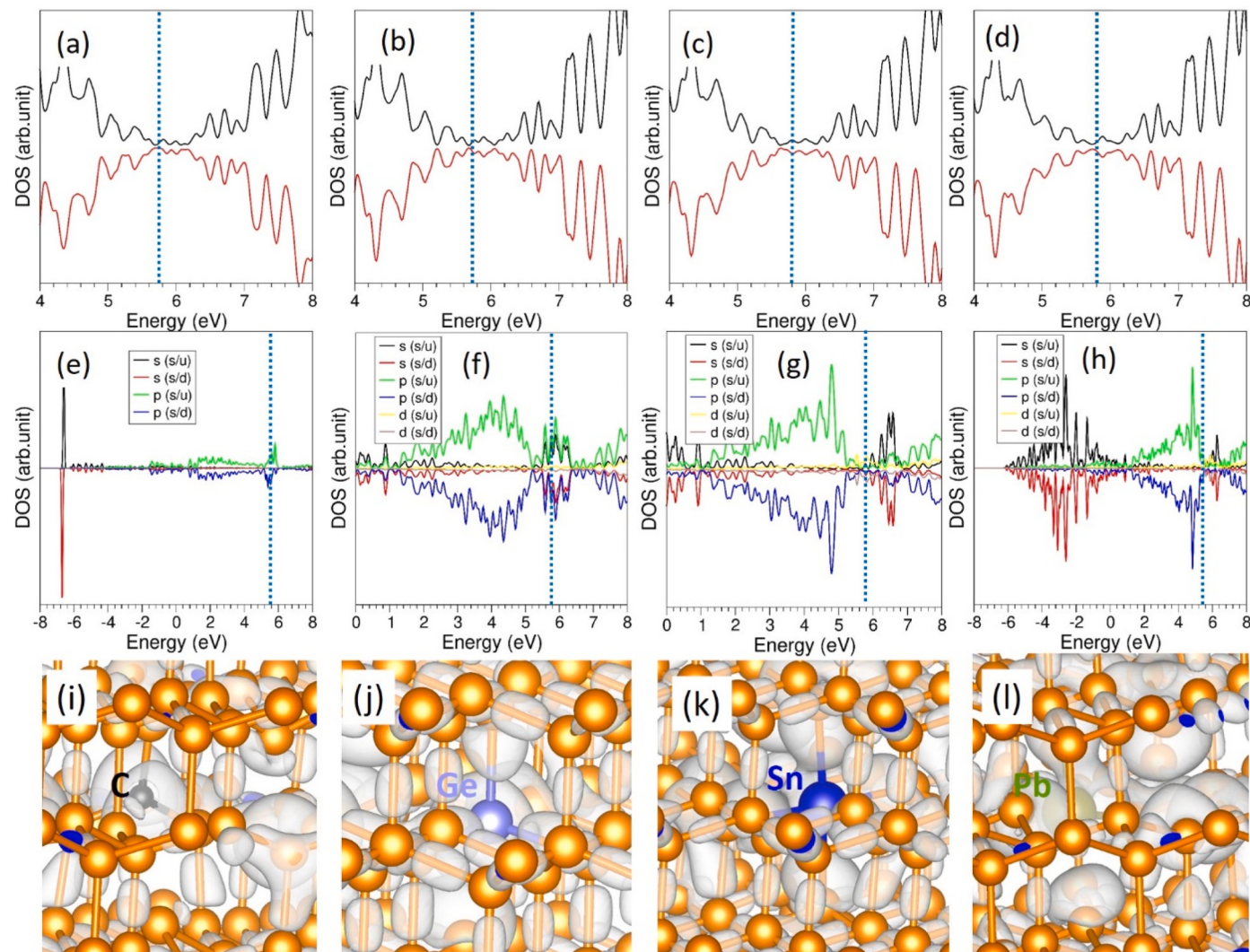


Fig. 7. Total DOS plots of (a) V GeV, (c) $VSnV$ and (d) $VPbV$ defect clusters in Si. Corresponding atomic DOS plots (e–h) and charge density plots (i–l) associated with the states near the Fermi energy level are also shown.

Funding

The author(s) received no financial support for the research.

Declaration of competing interest

The authors declare that they have no known competing financial interests or personal relationships that could have appeared to influence the work reported in this paper.

Data availability

No data was used for the research described in the article.

Acknowledgement

We acknowledge the computational facilities and support provided by High Performance Computing Center at Imperial College London.

Appendix A. Supplementary data

Supplementary data to this article can be found online at <https://doi.org/10.1016/j.physb.2023.415540>.

References

- [1] A.H. Atabaki, S. Moazeni, F. Pavanello, H. Gevorgyan, J. Notaros, L. Alloatti, M. T. Wade, C. Sun, S.A. Kruger, H. Meng, K. Al Qubaisi, I. Wang, B. Zhang, A. Khilo, C.V. Baiocco, M.A. Popović, V.M. Stojanović, R.J. Ram, *Nature* 556 (2018) 349.
- [2] V. Adinolfi, E.H. Sargent, *Nature* 542 (2017) 324.
- [3] L.C. Andreami, A. Bozzola, P. Kowalczewski, M. Liscidini, L. Redorici, *Adv. Phys. X* 4 (2019), 1548305.
- [4] L.R. Schreiber, H. Bluhm, *Science* 359 (2018) 393.
- [5] D. Yang (Ed.), *Handbook of Photovoltaic Silicon*, Springer-Verlag GmbH Germany, part of Springer Nature, 2019.
- [6] X. Yu, J. Chen, X. Ma, D. Yang, *Mater. Sci. Eng. R* 74 (2013) 1–33.
- [7] P. Pichler, Intrinsic point defects, impurities, and their diffusion in silicon, in: S. Selberherr (Ed.), *Computational Microelectronics*, Springer-Verlag/Wien, 2004, pp. 281–329.
- [8] C.A. Londos, A. Chroneos, E.N. Sgourou, I. Panagiotidis, T. Angeletos, M. Potsidi, *Appl. Sci.* 12 (2022) 851.
- [9] J. Chen, X. Ma, D. Yang, *Solid State Phenom.* 156–158 (2010) 261.
- [10] J. Chen, D. Yang, *Phys. Status Solidi C* 6 (2009) 625.
- [11] J. Vanhellemont, X. Zhang, W. Xu, J. Chen, X. Ma, D. Yang, *J. Appl. Phys.* 108 (2010), 123501.
- [12] C. Achilli, N. Marini, G. Onida, T. Shinada, T. Tanii, E. Prati, *Scientif. Rep.* 8 (2018), 18054.
- [13] A. Chroneos, A.W. Grimes, H. Bracht, *J. Appl. Phys.* 105 (2009), 016102.
- [14] J. Chen, T. Wu, M. X. L. Wang, D. Yang, *J. Appl. Phys.* 103 (2008), 123519.
- [15] H. Li, D. Yang, X. Ma, X. Yu, D. Que, *J. Appl. Phys.* 96 (2004) 4161.
- [16] J. Chen, D. Yang, H. Li, X. Ma, D. Que, *J. Appl. Phys.* 99 (2006), 073509.
- [17] A. Chroneos, C.A. Londos, E.N. Sgourou, P. Pochet, *Appl. Phys. Lett.* 99 (2011), 241901.
- [18] C. Clays, E. Simoen, V.B. Neimash, A. Kraitchinskii, M. Kras'ko, O. Puzenko, A. Blondefel, P. Claws, *J. Electrochem. Soc.* 148 (2001) G738 b.
- [19] M. Kras'ko, A. Kolosiuk, V. Voitovych, V. Povarchuk, *Phys. Status Solidi* 218 (2021), 2100209.
- [20] A. Chroneos, C.A. Londos, E.N. Sgourou, *J. Appl. Phys.* 110 (2011), 093507.
- [21] W. Lan, Y. Sun, T. Zhao, D. Yang, X. Ma, *Silicon* 12 (2020) 1433.
- [22] W. Wijaranakula, *J. Appl. Phys.* 72 (1992) 2713.
- [23] C. Gao, X. Ma, J. Zhao, D. Yang, *J. Appl. Phys.* 113 (2013), 093511.
- [24] G. Watkins, *Phys. Rev. B* 12 (1975) 751.
- [25] M. Funicelli, J.R. Byberg, *Phys. Rev. B* 61 (2000) 2657.
- [26] M. Funicelli, J.R. Byberg, *Physica B* 273–274 (1990) 524.
- [27] A. Brelo, *IEEE Trans. Nucl. Sci.* 19 (1972) 220.
- [28] K.L. Brower, *Radiat. Eff.* 8 (1971) 213.
- [29] M. Kaukonen, R. Jones, S. Oberg, P.R. Briddon, *Phys. Rev. B* 64 (2001), 245213.
- [30] M. Kaukonen, R. Jones S. Oberg, P.R. Briddon, *Nucl. Instrum. Methods Phys. Res. B* 186 (2002) 24.
- [31] L.I. Khirunenko, O.O. Kobzar, Yu V. Pomozov, M.G. Sosnin, M.O. Tripachko, *Physica B* 340–342 (2003) 541.
- [32] W. Wijaranakula, *J. Appl. Phys.* 69 (1991) 2737.
- [33] G. Watkins, *Phys. Rev. B* 12 (1975) 4383.
- [34] A. Nylandsted Larsen, J.J. Coubet, P. Mejilholm, J. Sherman Christensen, M. Funicelli, H.P. Gunnlaugsson, G. Weyer, J. Wulff Petersen, A. Resende, M. Kaukonen, R. Jones, S. Oberg, P.R. Briddon, B.G. Svensson, J.L. Lindstrom, S. Dannefaer, *Phys. Rev. B* 62 (2000) 4535.
- [35] C.V. Budtz-Jørgensen, P. Kringsjø, A. Nylandsted Larsen, N.V. Abrosimov, *Phys. Rev. B* 58 (1998) 1110.
- [36] A. Brelo, in: J.E. Whitehouse (Ed.), *Radiation Damage and Defects in Semiconductors* (Inst. Phys. Conf. Ser. No 16), Institute of Physics Publishing, London, 1973, p. 191.
- [37] A. Chroneos, E.N. Sgourou, C.A. Londos, U. Schwingenschlogl, *Appl. Phys. Rev.* 2 (2015), 021306.
- [38] M.L. David, E. Simoen, C. Clays, V. Neimash, M. Kras'ko, A. Kraitchinskii, V. Voitovych, A. Kabaldin, J.F. Barbot, *J. Phys. Condens. Matter* 17 (2005) S2255.
- [39] M.L. David, E. Simoen, C. Clays, V. Neimash, M. Kras'ko, A. Kraitchinskii, V. Voitovych, A. Kabaldin, J.F. Barbot, *Solid State Phenom.* 108–109 (2005) 373.
- [40] C.A. Londos, D. Aliprantis, E.N. Sgourou, A. Chroneos, P. Pochet, *J. Appl. Phys.* 111 (2012), 123508.
- [41] H. Hohler, A. Atodirasei, k. Schroeder, R. Zeller, P.H. Deterichs, *Phys. Rev. B* 71 (2005), 035212.
- [42] E.N. Sgourou, D. Timerkaeva, C.A. Londos, D. Aliprantis, A. Chroneos, D. Caliste, P. Pochet, *J. Appl. Phys.* 113 (2013), 113506.
- [43] H. Wang, A. Chroneos, C.A. Londos, E.N. Sgourou, U. Schwingenschlogl, *Phys. Chem. Chem. Phys.* 16 (2014) 8487.
- [44] V.B. Neimash, V. Voitovych, M.M. Kras'ko, A. Kraitchinskii, O.M. Kabaldin, Y. V. Pavlovskyi, V.M. Tsmots, *Ukrainian J. Phys.* 50 (2005) 1273.
- [45] V.B. Neimash, V. Voitovych, A.M. Kraitchinskii, L.I. Shpinar, M.M. Kras'ko, V. M. Popov, A.P. Pokanevych, M.I. Gorodyskyi, Y.V. Pavlovskyi, V.M. Tsmots, *Ukrainian J. Phys.* 50 (2005) 492.
- [46] J. Chen, X. Ma, D. Yang, *Solid State Phenom.* 156–158 (2010) 261.
- [47] K. Milands, J. Verheyden, T. Banancira, W. Deweerdt, H. Pattyn, S. Buckhpan, D. L. Williamson, F. Varmeren, G. Van Tendeleo, C. Vlekken, S. Libbrechtand, C. Van Haeserdonck, *J. Appl. Phys.* 81 (1997) 2148.
- [48] C.A. Londos, E.N. Sgourou, D. Hall, A. Chroneos, J. Mater. Sci. Mater. Electron. 25 (2014) 2395.
- [49] K. Sueoka, E. Kamiyama, J. Vanhellemont, *J. Appl. Phys.* 114 (2013), 153510.
- [50] G. Davies, R.C. Newman, Carbon in monocrystalline silicon, in: T.S. Moss (Ed.), *Handbook on Semiconductors*, vol. 3, Elsevier Science B.V., 1994, p. 1357.
- [51] A. Borghesi, B. Pivac, A. Sasselass, A. Stella, *J. Appl. Phys.* 77 (1995) 4169.
- [52] H. Bender, J. Vanhellemont, in: S. Mahajan (Ed.), *Handbook on Semiconductors*, vol. 3, Elsevier Science, 1994, p. 1637.
- [53] C.A. Londos, M.S. Potsidi, V.V. Emtevsev, *Phys. Stat. Sol. (c)* 2 (2005) 1963.
- [54] D. Yang, J. Chen, X. Ma, D. Que, *J. Cryst. Growth* 311 (2009) 837.
- [55] V.V. Voronkov, R. Falster, C.A. Londos, E.N. Sgourou, A. Andrianakis, H. Ohyama, *J. Appl. Phys.* 110 (2011), 093510.
- [56] E.V. Lavrov, M. Fanciulli, M. Kaukonen, R. Jones, P.R. Briddon, *Phys. Rev. B* 64 (2001), 125212.
- [57] A. DalPino Jr., A.M. Rappe, J.D. Ioannopoulos, *Phys. Rev. B* 47 (1993), 12554.
- [58] T. Terhoff, *Phys. Rev. Lett.* 64 (1990) 1757.
- [59] F.S. Gentile, A. Platonenko, K.E. El-Kelany, M. Rerat, P. D'Arco, R. Dovesi, *J. Comput. Chem.* 41 (2020) 1638.
- [60] A. Bean, R.C. Newman, R. Smith, *J. Phys. Chem. Solid.* 31 (1970) 739.
- [61] A.V. Drurechenskil, A.A. Karanovich, B.P. Kashnicov, *Sov. Phys. Semicond.* 21 (1987) 29.
- [62] C.A. Londos, G. Antonaras, A. Chroneos, J. Mater. Sci. Mater. Electron. 24 (2013) 4328.
- [63] E.G. Sieverts, J.W. Corbett, *Solid State Commun.* 43 (1982) 41.
- [64] P. Pichler, Intrinsic point defects, impurities, and their diffusion in silicon, in: S. Selberherr (Ed.), *Computational Microelectronics*, Springer-Verlag/Wien, 2004, pp. 331–467.
- [65] G. Kresse, J. Furthmüller, *Phys. Rev. B* 54 (1996) 11169–11186.
- [66] P.E. Blöchl, *Phys. Rev. B* 50 (1994) 17953–17979.
- [67] J.P. Perdew, K. Burke, M. Ernzerhof, *Phys. Rev. Lett.* 77 (1996) 3865–3868.
- [68] H.J. Monkhorst, J.D. Pack, *Phys. Rev. B* 13 (1976) 5188–5192.
- [69] W.H. Press, S.A. Teukolsky, W.T. Vetterling, B.P. Flannery, *Numerical Recipes in C* (2nd ed.): the Art of Scientific Computing, Cambridge University Press, 1992.
- [70] G. Henkelman, A. Arnaldsson, H. Jónsson, *Comput. Mater. Sci.* 36 (2006) 354–360.
- [71] S. Kavita, M. Alagusundarya, V.V. Ramakrishna, V. Suresh, P. Bhatt, P. Srimathi, R. Archana, D. Kar, T. Thomas, R. Gopalan, *J. Alloys Compd.* 895 (2022), 162597.
- [72] W. Bludau, A. Onton, W. Heinke, *J. Appl. Phys.* 45 (2003) 1846–1848.
- [73] Z.-h. Yang, H. Peng, J. Sun, J.P. Perdew, *Phys. Rev. B* 93 (2016), 205205.
- [74] M. Hu, Z. Wang, Y. Xu, J. Liang, J. Li, X. Zhu, *Phys. Chem. Chem. Phys.* 20 (2018) 26091–26097.
- [75] M. Rahm, R. Hoffmann, N.W. Ashcroft, *Chem. Eur. J.* 22 (2016) 14625–14632.
- [76] W.C. Martin, R.W. Wiese, Atomic spectroscopy, in: G.W.F. Drake (Ed.), *Atomic, Molecular, & Optical Physics Handbook*, AIP, Woodbury, NY, 1996, pp. 135–153 (Chapter 10).
- [77] A. Chroneos, *J. Appl. Phys.* 105 (2009), 056101.
- [78] A. Chroneos, R.W. Grimes, H. Bracht, *J. Appl. Phys.* 106 (2009), 063707.
- [79] A. Chroneos, C. Jiang, R.W. Grimes, U. Schwingenschlögl, H. Bracht, *Appl. Phys. Lett.* 95 (2009), 112101.
- [80] A. Chroneos, D. Skarlatos, C. Tsamis, A. Christofi, D.S. McPhail, R. Hung, *Mater. Sci. Semicond. Process.* 9 (2006) 640–643.
- [81] S. Dev, M. Pradhan, N. Variam, S. Lodha, *IEEE Trans. Electron. Dev.* 67 (2020) 419–423.